Architecture of the Human Urotensin II Receptor: Comparison of the Binding Domains of Peptide and Non-Peptide Urotensin II Agonists

Antonio Lavecchia,* Sandro Cosconati, and Ettore Novellino*

Dipartimento di Chimica Farmaceutica e Tossicologica, Università di Napoli "Federico II", Via D. Montesano 49, 80131 Napoli, Italy

Received November 4, 2004

The human urotensin II receptor (*h*-UTR) is a member of the family of rhodopsin-like G-protein-coupled receptors (GPCRs) involved in the modulation of the functionality of many tissues and organs. Recently the urotensin-II (UII) neuropeptide, which is a potent vasoconstrictor in mammals and it is postulated to play a central role in cardiovascular homeostasis, has been identified as an agonist of the UII receptor. To elucidate the receptor's molecular recognition, a *h*-UTR model was constructed by homology modeling using the 2.6 Å crystal structure of bovine rhodopsin as a template and subsequently refined by molecular dynamics simulations. The molecular recognition of *h*-UTR was probed by automated docking of P5U, a potent UII peptide agonist, as well as of the non-peptide compounds **1**−**4**. We believe that this new model of the *h*-UTR provides the means for understanding the ligand's potency and for facilitating the design of novel and more potent UII ligands.

Introduction

Urotensin II (UII), a urophysial peptide, was first characterized biologically by Bern et al. in 1967.[1] Although this cyclic dodecapeptide (AGTADCFWKYCV) had initially been isolated from the goby *Gillichthys mirabilis*, the cDNA encoding its precursor has now been sequenced from many species, including humans.[2−4] The composition of UII ranges from 11 amino acids in humans to 14 amino acids in mice, always with the conserved cysteine-linked macrocycle CFWKYC, which is essential for the biological activity.[5] In situ hybridization and immunohistochemistry have revealed that human UII is not only localized to the medulla oblongata of the brain and the spinal cord in the central nervous system but is also present in such tissues as adrenal glands, kidney, and spleen, suggesting neurohormonal or hormonal properties.[2,6] UII appears to be the most potent vasoconstrictor known up to now,[7−9] causing concentration-dependent contraction of isolated arterial rings of rats and humans with an EC_{50} value of less than 1 nM, which means it is about 10 times more potent than endothelin 1. However, the in vivo effects of UII can be tissue- and species-specific, and sometimes contradictory. Recent studies, in fact, describe how human UII has potent vasodilator and cardiostimulant responses in human tissues.[10,11] In addition, this peptide has been recently reported to induce hypertrophy in cardiomyocytes[12] and proliferation of smooth muscle cells,[13] which suggests a possible involvement in heart failure and atherosclerosis.

Recently, it has been shown that human UII is the endogenous ligand of a G-protein-coupled receptor (GPCR),[3] which was isolated from a human genomic library[6] and which possessed high sequence similarity to GPR14, an orphan receptor identified in rat[14] and currently referred to as the UT receptor. The human UII receptor (*h*-UTR) belongs to class A, the rhodopsin-like family, of the peptide subfamily of GPCRs and is comprised of 389 residues (386 for the rat UII receptor).[3] A schematic representation of the *h*-UTR is given in Figure 1. The receptor possesses two potential N-glycosylation sites in the N-terminal domain (Asn29 and Asn33) and two cysteine residues in the first and second extracellular loop, which are thought to participate in disulfide bonding. Intracellular portions contain the Glu/Asp-Arg-Tyr motif, which is well-conserved among GPCRs, and potential phosphorylation sites are found in the cytoplasmic tail.

Thus, the UII/UTR biological system exhibits a remarkable potential for the development of novel therapeutic strategies, especially those related to the treatment of cardiovascular diseases. Such developments require a precise knowledge of the pharmacophoric elements within UII essential for the affinity and the activity of this peptide.

Structure−activity relationship (SAR) studies revealed that the cyclic portion (Cys5−Cys10) of the peptide is crucial for biological activity, and the sequence Trp7-Lys8-Tyr9 has been shown to be the most important for *h*-UTR occupation and activation.[15,16] The replacement of Lys8 with Orn8 leads to the identification of the low potency UTR partial agonist [Orn^8]UII.[17] In addition, replacement of Cys5 with penicillamine in the octapeptide UII(4−11) generated [Pen^5]UII(4−11)[18] (P5U in Chart 1), which behaves as a potent UTR agonist and shows higher affinity (EC_{50} = 0.2 nM) than human UII at cloned *h*-UTRs as well as higher activity in the rat thoracic aorta assay.

The first non-peptide UTR agonist reported in the literature, compound AC-7954 (**1**, Chart 2), has been identified by high-throughput screening of a combinatorial library of small organic molecules and showed an EC_{50} of 300 nM at the *h*-UTR.[19] Later on, the dihydropyrazole **2** turned out to have agonist activity toward *h*-UTRs (EC_{50} = 4.0 μM) when tested with the functional

* To whom correspondence should be addressed. Tel: ++39 081 678613. Fax: ++39 081 678644. E-mail: lavecchi@unina.it and novellin@unina.it.

10.1021/jm049110x CCC: $30.25
Published on Web 02/22/2005

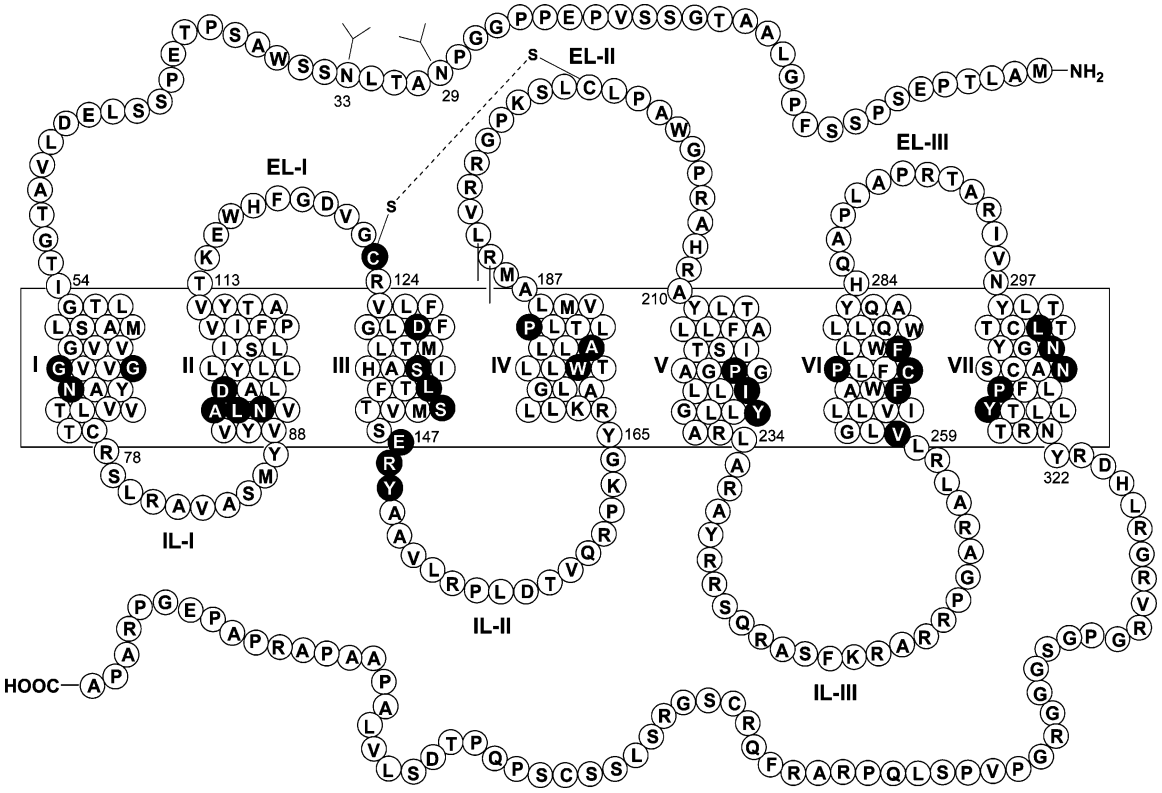

Figure 1. Serpentine model of the *h*-UTR sequence. The black lines represent the boundaries of the membrane. Filled circles indicate the residues highly conserved among the GPCRs superfamily. The TM helices are denoted by roman numerals. The arabic numbers indicate the position of the residues inside the TM domain. The glycosilation site on the ELII is also shown. IL = intracellular loop and EL = extracellular loop.

Chart 1

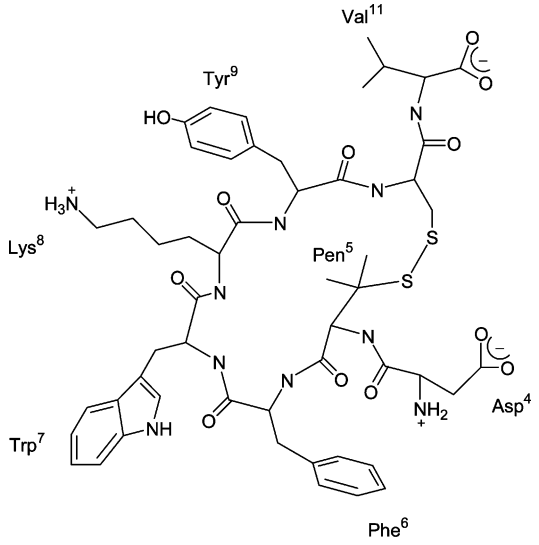

P5U

Chart 2

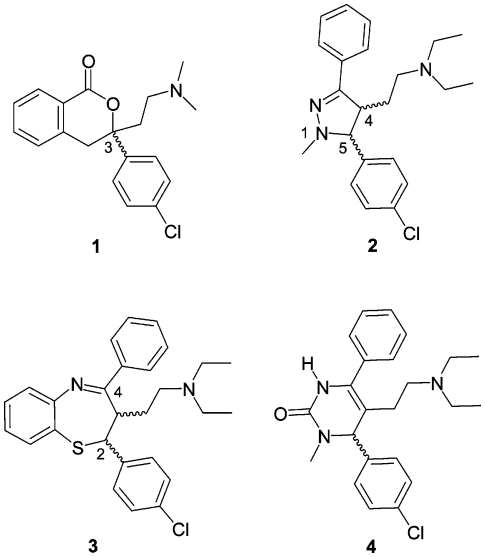

mammalian cell-based R-SAT assay.[20] In the same study, the dihydrobenzothiazepine **3** and the dihydropyrimidinone **4** have also been found to be active on the *h*-UTRs with EC_{50} values of 6.3 and 5.0 μM, respectively.

In addition to the SARs of the UII ligands, structural knowledge of their target receptor protein is important in facilitating drug design. Recently, the ground-state X-ray structure of bovine rhodopsin (*b*-Rho) with 2.8-Å resolution[21] has advanced our understanding of the structure and activation of GPCRs. This crystal structure can be used as a structural template to model the transmembrane domain of other family A GPCRs.[22] Ballesteros et al.[23] demonstrated that GPCRs maintain their general folding characteristics by means of structural mimicry, despite the possible low homology between these receptors. This structural mimicry also enables localized variations within the binding sites of the receptors that are responsible for the selectivity of a receptor toward a diverse group of ligands. However, Ballesteros and co-workers emphasize that substantial modifications of the initial template may be required to refine the particular conformation of the binding site

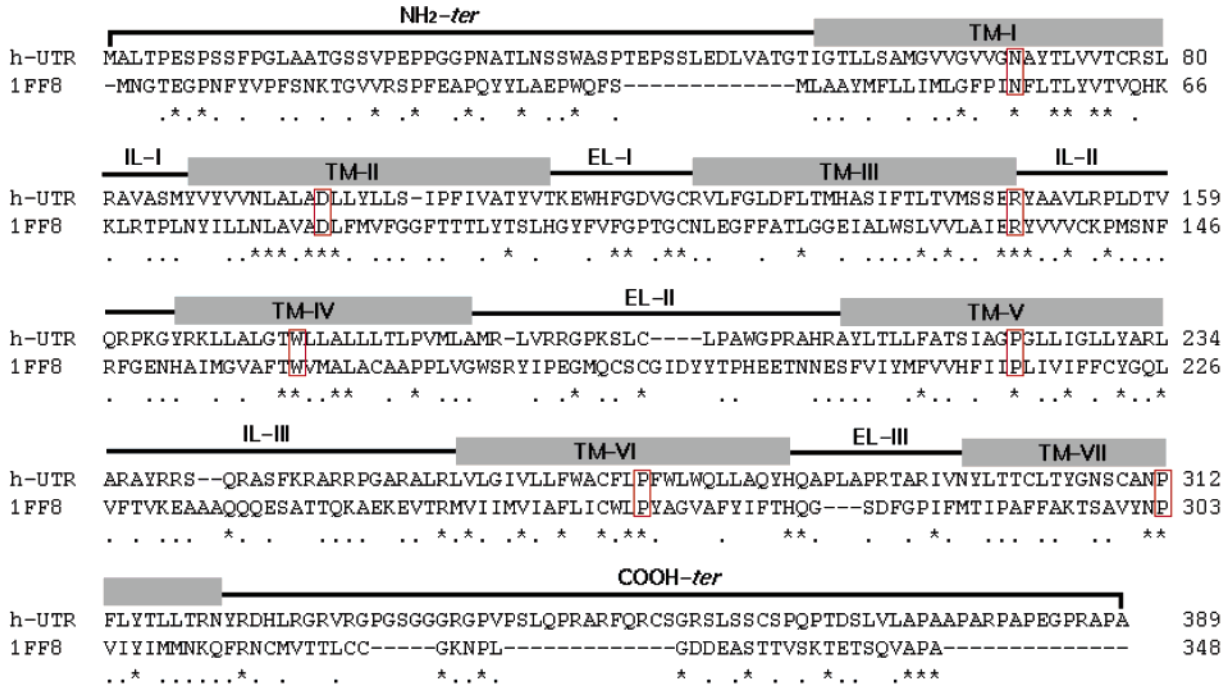

Figure 2. Pairwise alignment of *h*-UTR and *b*-Rho (1F88). The conserved key residues used to align the sequences are shown in red boxes. In all sequence alignment figures, an asterisk (*) indicates an identical amino acid; quotation marks indicate a "conserved" amino acid, which meets the criteria for either highly conservative substitutions or semiconservative substitutions, as defined by CLUSTALW.

for the exploration of specific ligand−receptor interactions. A study by Bissanz and co-workers[24] demonstrated that comparison (or homology) models of GPCRs can also be used as suitable targets for protein-based virtual screening of chemical databases.

In the present work, with the aim of gaining a better understanding of the ligand/*h*-UTR interactions and, in particular, to outline specific UII agonists binding mode, a theoretical model of the *h*-UTR, developed by comparative modeling from the crystallographic structure of *b*-Rho,[21] is presented. This model, refined on the basis of the actual knowledge derived from site-directed mutagenesis experiments and the biophysical data obtained from rhodopsin-like receptors, has been employed for extensive docking studies of peptide and nonpeptide UII agonists (Charts 1 and 2). The results are compared with SARs data to identify key ligand/receptor interactions involved in the molecular recognition process. The correct overlay of these interactions will provide a steady basis for rational design of new UII agonists.

Results and Discussion

The three-dimensional model of the transmembrane domain of the *h*-UTR (Figure 1) was constructed by computer-aided model-building techniques from the transmembrane domain of the recently reported crystal structure of *b*-Rho[21] (PDB entry code 1F88), a membrane protein belonging to the GPCRs superfamily. Conserved residues Asn55 (residue number in the PDB file of *b*-Rho) and Asn69 (residue number in the *h*-UTR sequence), Asp83 and Asp97, Arg135 and Arg148, Trp161 and Trp174, Pro215 and Pro223, Pro267 and Pro273, and Pro303 and Pro312 were employed in the alignment of *b*-Rho and *h*-UTR transmembrane sequences. The sequence alignment of *h*-UTR and *b*-Rho, shown in Figure 2, highlights a significant sequence identity in the transmembrane (TM) regions of the two proteins. The percentage identities (and similarity—identical plus conservative substitutions) for each of the seven transmembrane regions are TMI, 24% (60%); TMII, 23% (58%); TMIII, 17% (63%); TMIV, 22% (61%); TMV, 20% (68%); TMVI, 27% (54%); and TMVII, 12% (69%).

The loop search algorithm available within SYBYL[25] was used to search the binary protein database in this program package for suitable protein fragments. The templates for each of the extracellular loops (ELs) were identified according to the following criteria: (1) the sequence in the template protein had to be of a length comparable to that of the target loop, (2) the template structure had to be a loop structure, (3) the template structure had to form a loop between two antiparallel helical elements, (4) the distance between the ends of the loop in the template structure had to differ by no more than 1 Å from the distance between the TM segment to be connected in the target protein, and (5) the sequence identity of the template protein with the target protein had to be ≥20%. For each loop only one potential template structure was identified in the PDB that met these stringent criteria. The templates used were as follows: ELI was modeled on 1JTB, which is a lipid transfer protein structure;[26] ELII was modeled on 1BVP, which is a viral structure;[27] ELIII was modeled on 1NAL, which is a *N*-acetylneuraminate lyase structure.[28] All loop regions used were checked to confirm that the loops were well ordered (low *B* factors and full occupancies) in the template structure.

Most GPCRs of the rhodopsin family have a disulfide bridge between TMIII and ELII.[29] In *b*-Rho, this bridge draws the ELII loop down so that the loop covers the

ligand-binding site and, thus, is involved in ligand recognition. In *h*-UTRs, this particular disulfide bridge is hypothesized between the highly conserved Cys123 in ELI and the Cys199 in ELII, respectively. Accordingly, the present model includes this disulfide linkage, which is located near the ligand-binding site.

The molecular dynamics (MD) simulation of the *h*-UTR model was stable, as there was no drift in the energy or temperature. The root-mean-squared deviation (rmsd) of the protein backbone was monitored over the simulation time for the *h*-UTR model after a least-squares fit to the initial structure. Even though the deviation increases to about 2 Å, the receptor structure remained stable.

It is a well-known fact that *b*-Rho was crystallized in its inactive state, that conformationally differs from the activated state.[21] Therefore, it may be assumed that the initial *h*-UTR model is closer to its inactive form than to its activated, agonist-bound state. Until now, there is only a crude picture of the conformational changes that occur during receptor activation. Recent studies based on electron paramagnetic resonance and fluorescence spectroscopy[30] suggest an outward movement of the cytoplasmic end of TMIII and TMVI,[31,32] as well as an anticlockwise rotation of TMVI around its helical axis when viewed from the extracellular side. Other helices probably adjust their positions upon activation as well. Moreover, in a UV absorption study,[33] it was suggested that when rhodopsin is activated, the aromatic residue Trp265 in TMVI (corresponding to Phe271 in *h*-UTR) is proposed to undergo a rotameric shift of the $\chi 1$ torsion angle from gauche$^+$ to trans. Thus, the intramolecular contact network might be destabilized, facilitating the conformational change to activate the receptor. Very recently Nikiforovich and Marshall proposed a three-dimensional model for meta-II rhodopsin featuring a similar change to the conformation of Trp265.[34] Interestingly, this rotamer switch was also confirmed in the present study. Before the MD simulation, Phe271 (Trp265 in *b*-Rho) was in the gauche$^+$ $\chi 1$ configuration, as in the rhodopsin template. During the MD simulation of the *h*-UTR model, the rotamer of Phe271 shifted from gauche$^+$ $\chi 1$ to trans $\chi 1$. For our purposes, although we do not wish to neglect this dynamical feature of the GPCR structure, in the absence of a crystal structure of a representative GPCR, we prefer not to let our results become biased by a purported structure that may turn out to be inaccurate. For example, in the study proposing homology models in the activated state,[24] there was a need to expand the size of the ligand-binding pocket to accommodate agonists. Even if feasible, there is no evidence to support such a decision. In any case, it has been shown that, while there are indeed certain conformational adjustments to the structure, both in the backbone and in side chains, there are only very few changes in the residues that actually participate in ligand recognition.[35] This further justifies our choice of a knowledge-based docking approach where experimental facts concerning the ligand moieties and the residues involved are used, rather than a method based on a molecular mechanical force field. The latter requires an accurate structure for the receptor and not one that has been adjusted according to purely qualitative criteria.

To validate the reliability of the calculated model, the program PROCHECK,[36,37] which automatically checks the stereochemical accuracy, packing quality, and folding reliability, was employed. Using a Ramachandran plot, φ and ψ angles were compared with the rhodopsin crystal structure. All amino acids in the α-helices were located in the favored region of the right-handed α-helix in the Ramachandran plot. From calculated ω angles, there were no cis peptide bonds in the calculated *h*-UTR model as well as in *b*-Rho structure. All Cα atoms except Cys displayed *S*-chirality. For the packing quality, there were no bump regions in the calculated *h*-UTR model. Figure 3 presents the final *h*-UTR model compared with the *b*-Rho crystal structure. The secondary structures were assigned as implemented by SYBYL. As expected, deviations from the ideal α-helical structure were located in the respective TM regions of both the receptors.

Network of Hydrogen Bonds. *b*-Rho Compared to *h*-UTR. The transmembrane region of *b*-Rho is stabilized by a number of interhelical hydrogen bonds and hydrophobic interactions, most of which are mediated by highly conserved residues in GPCRs.[21] For example, in the case of the unoccupied *h*-UTR, the carboxylate group of Asp97 (TMII) interacted with Asn69 (TMI) and Asn311 (TMVII), as was observed in *b*-Rho, which had interhelical hydrogen bonds between the highly conserved Asn55 (TMI) and the backbone carbonyl groups of Asn299 (TMVII) and Asp83 (TMII). Another Asn residue, Asn78 (TMII), in *b*-Rho formed hydrogen bonds to Ser127 (TMIII), Thr160 (TMIV), and Trp161 (TMIV). The corresponding amino acid in the *h*-UTR, Asn92 (TMII), showed the same hydrophilic interactions with Thr140 (TMIII), Thr173 (TMIV), and Trp174 (TMIV). With respect to the highly conserved (D/E)R(Y/W) motif in GPCRs, the carboxylate of Glu134 (TMIII) in *b*-Rho formed a salt bridge with the guanidinium group of the adjacent Arg135 (TMIII). An analogous interaction occurred in the *h*-UTR, i.e., the salt bridge of Arg148 (TMIII) with Glu147 (TMIII). For the NPXXY motif in the TMVII of GPCRs, the hydroxyl group of Tyr306 (TMVII) was close to Asn73 (TMII) in *b*-Rho, which was also highly conserved among GPCRs. The same result appeared with the calculated UTR structure, i.e., the OH group of Tyr315 (TMVII) was located in proximity to the side chain of Asn92 (TMII).

Other important interhelical hydrogen-bonding interactions for highly conserved sequences took place in *h*-UTR. Table 1 details the interhelical hydrogen bonds computed over the minimized average structure of the protein. In this table, residues highly conserved in GPCRs are in bold.

Hydrophobic Interactions. The seven-helical bundle is stabilized by a network of π-stacking interactions involving a number of residues highly conserved in GPCRs, such as Phe267 (TMVI), Trp268 (TMVI), Phe271 (TMVI), Phe274 (TMVI), Trp275 (TMVI), and Tyr305 (TMVII). Phe271 in helix VI corresponds to Trp265 in *b*-Rho, which is highly conserved within the large group of the rhodopsin-like receptors, and it appears likely to play a crucial role in receptor activation for many GPCRs. Consequently, in *h*-UTR, the aromatic amino acid Phe271 might be able to fulfill the same role as tryptophan. Among hydrophobic interactions, the con-

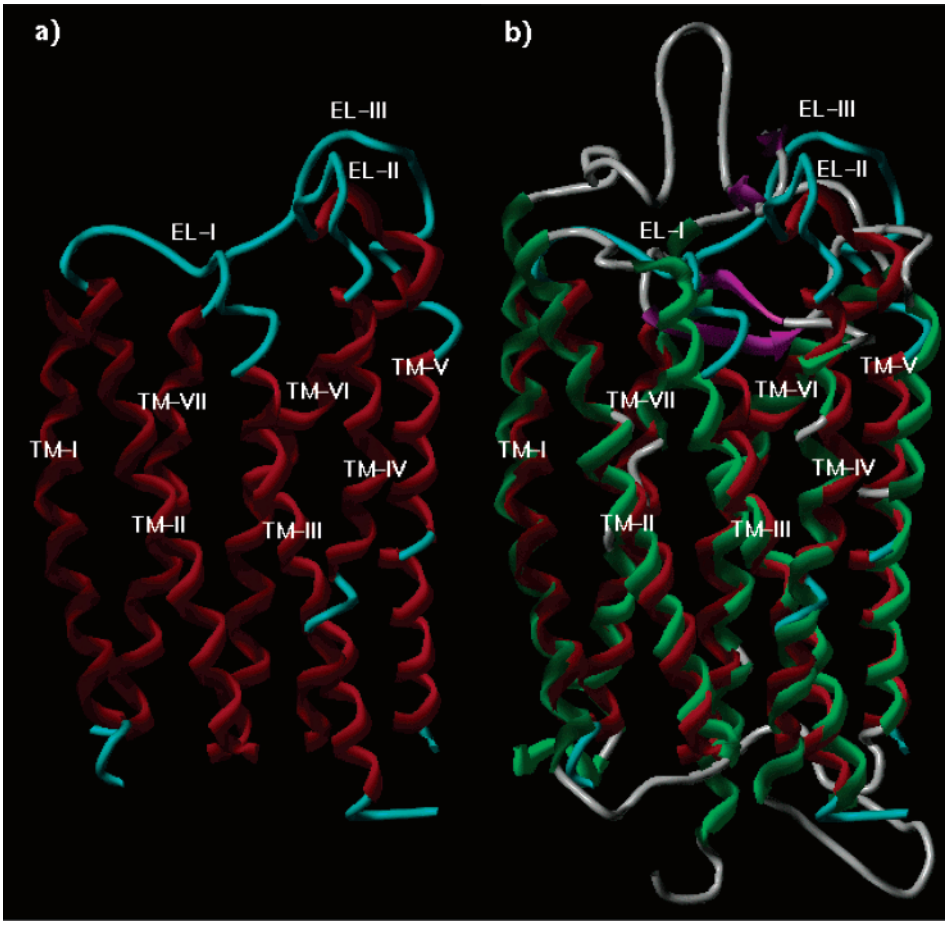

Figure 3. *h*-UTR model compared with the *b*-Rho crystal structure. Secondary structure coding: α-helix, red (*h*-UTR)/green (*b*-Rho); *β*-sheet, magenta; other, cyan (*h*-UTR)/white (*b*-Rho): (a) *h*-UTR model and (b) *h*-UTR model superimposed with *b*-Rho.

Table 1. Geometries of the Interhelical Hydrogen Bonds in the Model of *h*-UTR

residue[a]	acceptor[b] (A)	residue[a]	donor[b] (D)	H−A[c] (Å)	D−H−A[d] (deg)
Val112 (TMII)	O	Thr56 (TMI)	$O^{\gamma}H$	2.1	151
Glu147 (TMIII)	$O^{\epsilon 1}$	Tyr89 (TMII)	$O^{\gamma}H$	1.8	170
Asn92 (TMII)	$O^{\delta 1}$	Lys167 (TMIV)	$N^{\zeta}H$	2.3	133
Asn92 (TMII)	$O^{\delta 1}$	**Trp174** (TMIV)	$N^{\epsilon}H$	2.2	133
Thr140 (TMIII)	$O^{\delta 1}$	**Asn92** (TMII)	$N^{\delta 2}H$	2.3	125
Asp97 (TMII)	$O^{\delta 2}$	Thr133 (TMIII)	$O^{\gamma}H$	1.8	173
Asp97 (TMII)	$O^{\delta 1}$	**Asn69** (TMI)	$N^{\delta 2}H$	2.4	165
Asp97 (TMII)	$O^{\delta 1}$	**Asn311** (TMVII)	$N^{\delta 2}H$	2.8	158
Asp130 (TMIII)	$O^{\delta 1}$	Tyr305 (TMVII)	$O^{\gamma}H$	1.8	144
Asp130 (TMIII)	$O^{\delta 2}$	Tyr100 (TMII)	$O^{\gamma}H$	1.6	159
Glu147 (TMIII)	$O^{\epsilon 1}$	Tyr165 (TMIV)	$O^{\gamma}H$	1.6	170
Thr173 (TMIV)	O^{γ}	**Asn92** (TMII)	$N^{\delta 1}H$	2.4	163
Ser103 (TMII)	O^{γ}	Arg166 (TMIV)	$N^{\epsilon}H$	1.9	160

[a] Residues highly conserved in GPCRs are in bold. [b] Atom names of the amino acids are based on IUPAC nomenclature. [c] H−A is the hydrogen−acceptor distance. [d] D−H−A is the donor−acceptor angle.

served Phe271 was typically surrounded by hydrophobic residues from TMs III, VI, and VII, as was observed for another GPCR, the thyrotropin-releasing hormone receptor.[38] Those hydrophobic amino acids near Phe271 were Met134 (TMIII), Phe267, Trp268, Phe274, Trp275, and Tyr305.

Docking Studies. To investigate the ligand recognition site of the *h*-UTR, we undertook docking studies of the highly active peptide P5U (Chart 1) and non-peptide compounds **1**−**4** (Chart 2) using the above-described *h*-UTR model. Since the receptor structure is only a homology model and the currently available docking programs may not work very well for peptide compounds, manual docking was conducted for P5U. For docking experiments, the conformation in solution of the cyclic ligand as experimentally determined by NMR and subsequent molecular dynamics (MD) in solvent was used.[18] The following criteria were employed to achieve meaningful docking modes: (i) No steric clashes could happen between any atom. (ii) SAR data of UII-related peptides had to be well-interpreted by the docked structure. (iii) The positively charged amino group of Lys8 had to be close to and pointing in the direction of the carboxylate group of Asp130, which is conserved in many GPCRs and positioned in the TMIII region. Accordingly, mutation of this aspartate has been shown to diminish the binding of various protonated amine ligands in other receptor systems.[39,40]

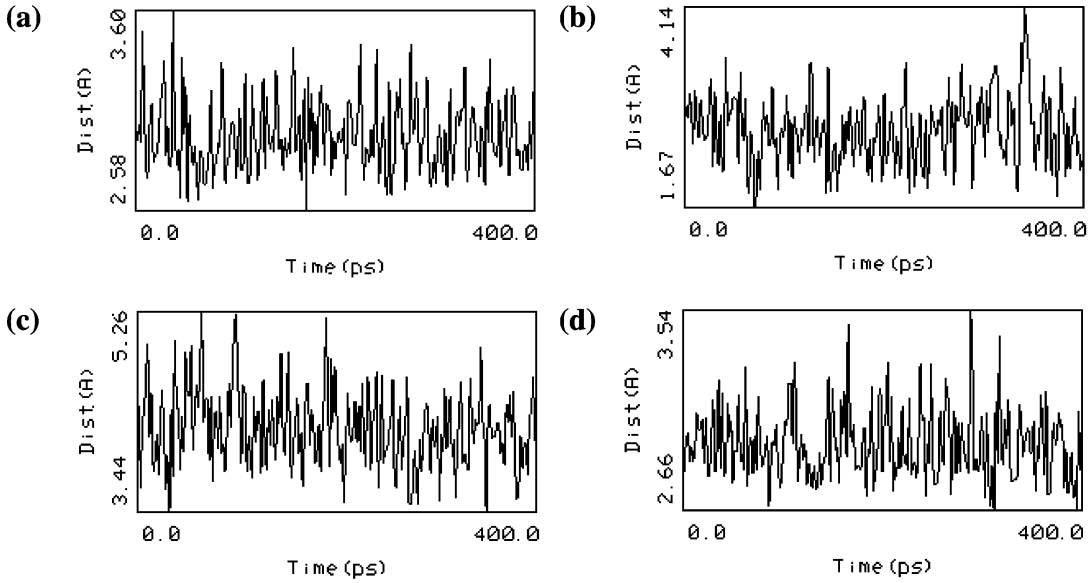

Figure 4. Results of MD simulations of *h*-UTR complexed with P5U. Graphics show plots of the monitored distance, in the complex, between the protonated N^{ϵ} of Lys8 in P5U and the O^{δ} of Asp130 (a), the OH oxygen of Tyr9 in P5U and the backbone CO oxygen of Ala281 (b), the Tyr9 phenolic ring center of mass of P5U and the Trp227 indole ring center of mass, (c) and the N^{ϵ} of Trp7 and backbone CO oxygen of Tyr298 (d).

To assess the stability of the P5U/*h*-UTR complex and to analyze the potential ligand/receptor interactions, energy minimization and MD simulations of 400 ps at a constant temperature of 300 K were run. During the MD simulation, the ligand and the amino acid side chains were allowed to relax, while the protein backbone was held frozen. The distances between the peptide and the key receptor residues were monitored along the complete 400 ps MD trajectory (Figure 4).

To inspect the variations in the ligand conformation, rmsd with respect to the starting structure was calculated. Interestingly, the rmsd of P5U backbone atoms turned out to be really stable throughout all the MD simulations ($0 < \text{rmsd} < 0.6$), indicating that the peptide settles into the receptor-binding site in a stable conformation.

As shown in Figure 5A, the hypothetical binding site of P5U is located among TMV, TMVI, TMVII, ELI, ELII, and ELIII. The binding mode of the peptide is determined mainly by the following interactions.

(i) An important feature of the P5U/*h*-UTR complex is the occurrence of a tight charge-reinforced hydrogen-bonding network involving the carboxylate group of Asp130 (TMIII) and the protonated ϵ-amino group of Lys8 of P5U, whose side chain is oriented along the receptor helical axis (Figure 5B). Such an interaction, which we assumed to be an anchoring point of the ligand to *h*-UTR, remained stable during the whole production run, as suggested by the trajectory plot in Figure 4a. It is worth noting that the protonated amino group of Lys8 forms another hydrogen bond with the backbone CO of Asp130, contributing to further stabilize the hydrogen-bonding pattern. Moreover, the above-mentioned network is further consolidated by two additional hydrogen bonds between the carboxylate of Asp130 and the OH group of both Tyr100 (TMII) and Tyr305 (TMVII) side chains. Inspection of the docked peptide ligand also reveals the presence of two other hydrogen bonds involving the indole NH of Trp277 and the backbone CO of both Lys8 and Trp7, respectively, of P5U. These results are in agreement with the SARs data indicating the importance of Lys8 in the receptor binding. In fact, Flohr et al. reported that replacement of this residue with Ala results in a peptide 6000-fold less active than the endogenous agonist UII.[16] (ii) A large hydrophobic pocket consisting of His208 (ELII), Leu212 (TMV), Trp277 (TMVI), Ala281 (TMVI), Gln285 (ELIII), and Val296 (ELIII) side chains hosts the aromatic ring of Tyr9 of P5U. The phenolic OH of this residue is close to hydrogen-bonding distance with the backbone CO of Ala281, which remains stable along the 400 ps MD trajectory (Figure 4b). In addition, the phenyl ring of Tyr9 appears to be optimally oriented for a π-stacking interaction with the aromatic indole system of Trp227. As shown in Figure 4c, the planes of the two aromatic rings are fairly parallel and separated by a distance ranging between 3.4 and 5.3 Å. The importance of Tyr9 in receptor binding has been underscored by SARs data. In fact, the exchange of Tyr9 by Ala resulted in a compound with no activity.[16] Moreover, Kinney et al. replaced this tyrosine with Phe to give rise a still active analogue, which suggests that the phenolic OH is not involved in receptor binding.[41] Still, substitution of Tyr9 with 2-Nal remarkably improved the affinity toward *h*-UTR, thus corroborating the idea that this residue interacts with the receptor through hydrophobic interactions. (iii) The indole system of Trp7 in P5U is sited in a large cleft made up by Gln53 (ELI), Ile54 (TMI), Gly55 (TMI), Tyr298 (TMVII), Leu299 (TMVII), Thr301 (TMVII), and Cys302 (TMVII) side chains. Within this pocket, the backbone CO of Tyr298 engages a hydrogen bond with the indole NH of Trp7. The trajectory plot of the analyzed complex in Figure 4d displays that this hydrogen bond turned out to be quite stable throughout the MD simulation. Our docking model is in accordance with the SAR data, which suggest that Trp7 interacts with the receptor with polar rather than hydrophobic interactions. In fact, the exchange of Trp7 by Ala or 2-Nal residues led to dramatic loss of potency and efficacy of the corresponding peptide.[16,41] (iv) For P5U,

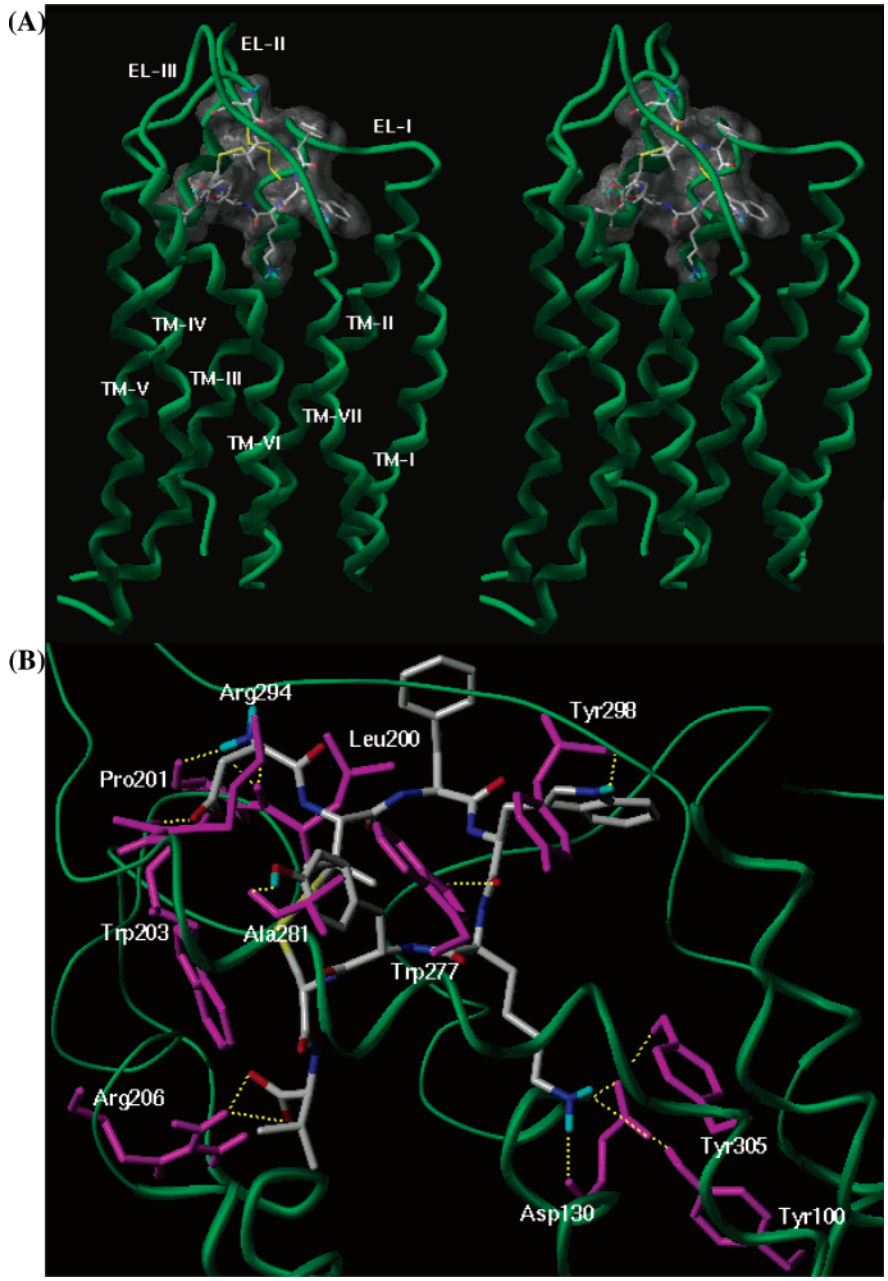

Figure 5. (A) Stereoview of the transmembrane domain of *h*-UTR. A translucent, reduced surface of the potent agonist P5U is displayed in white, indicating the region of the putative ligand-binding site. Receptor backbones are represented in green and labeled. The disulfide linkage between Cys123 in ELI and Cys199 in ELII is shown in yellow. (B) View of P5U within the binding pocket of *h*-UTR. The ligand is displayed in white, and key binding site residues are shown in magenta. Hydrogen bonds are represented with dashed yellow lines.

the Phe6 side chain points toward the external region of the receptor inserting between ELI and ELII to contact Val296 and Gln53 residues. This result still agrees with the SARs studies indicating that Phe6 plays a minor role in receptor binding, since its substitution with Ala results in a still full agonist peptide.[16] (v) The exocyclic carboxylate group of Asp4 in P5U, lying at the interface between ELII and ELIII, appears involved in a hydrogen-bonding network. Particularly, an oxygen of the carboxylate establishes a hydrogen bond with the backbone NH of Trp203 (ELII), while the other one forms two charge-reinforced hydrogen bonds with the guanidinium group of Arg294 (ELIII). In addition, the protonated N-terminal group of Asp4 engages two additional hydrogen bonds with the backbone CO of Pro201 and Leu200, respectively. All of the mentioned interactions are lost after 100 ps of MD simulations, thus explaining why the removal of the exocyclic Asp4 results in a still active compound.[42] (vi) The C-terminal Val11 of P5U is embedded within a hydrophobic cavity made up by the side chains of Phe131 (TMIII), Val184 (TMIV), Ala207 (ELII), Tyr211 (TMV), Leu212 (TMV), and Leu215 (TMV). Moreover, the negatively charged C-terminal group of Val11 establishes a salt bridge with the protonated guanidinium moiety of Arg206 (ELII).

As concerns the ligands **1**−**4**, docking experiments were carried out using the version 3.0.5 of the AutoDock program, which has been shown to successfully reproduce experimentally observed binding modes.[43,44] As shown in Table 2, the 50 independent docking runs performed for each ligand usually converged to a small number of different clusters ("clusters" of results dif-

Table 2. Result of 50 Independent Docking Runs for Each Ligand[a]

ligand	N_{tot}	f_{occ}	ΔG_{bind}	surrounding residues
(*R*)-**1**	11	15	−8.49	Val108 (TMII), Phe118 (ELI), Leu126 (TMIII), Phe127 (TMIII), **Asp130** (TMIII), Phe131 (TMIII), His208 (ELII), Leu212 (TMV), **Phe274** (TMVI), Trp277 (TMVI), Gln278 (TMVI), Arg294 (ELIII), Val296 (ELIII), Thr301 (TMVII), Cys302 (TMVII), Tyr305 (TMVII)
(4*R*,5*S*)-**2**	6	44	−8.72	Tyr100 (TMII), Phe118 (ELI), Leu126 (TMIII), Phe127 (TMIII), **Asp130** (TMIII), Phe131 (TMIII), Met134 (TMIII), His208 (ELII), Leu212 (TMV), Phe274 (TMVI), Trp277 (TMVI), Gln278 (TMVI), Ala 281 (TMVI), Gln282 (TMVI), Val296 (ELIII), Tyr298 (ELIII), Thr301 (TMVII), Cys302 (TMVII), Tyr305 (TMVII)
(*R*,*R*)-**3**	14	25	−8.58	Phe118 (ELI), Leu126 (TMIII), Phe127 (TMIII), **Asp130** (TMIII), Phe131 (TMIII), Met134 (TMIII), His208 (ELII), **Phe274** (TMVI), Trp277 (TMVI), Gln278 (TMVI), Gln285 (ELIII), Val296 (ELIII), Thr301 (TMVII), Cys302 (TMVII), Tyr305 (TMVII)
(*R*)-**4**	5	34	−7.78	Phe118 (ELI), Leu126 (TMIII), Phe127 (TMIII), **Asp130** (TMIII), Phe131 (TMIII), Met134 (TMIII), His208 (ELII), Leu212 (TMV), Leu215 (TMV), Phe271 (TMVI), **Phe274** (TMVI), Trp277 (TMVI), Gln278 (TMVI), Ala 281 (TMVI), Gln282 (TMVI), Val296 (ELIII), Tyr298 (ELIII), Thr301 (TMVII), Cys302 (TMVII), Tyr305 (TMVII)

[a] N_{tot} is the total number of clusters; the number of results in the top cluster is given by the frequency of occurrence, f_{occ}; ΔG_{bind} is the estimated free energy of binding for the top cluster results and is given in kcal/mol. The last column shows the contacting residues for the binding mode of the top cluster. Only residues within 4 Å from any atom of the docked ligands are shown. Highly conserved residues are highlighted in bold.

fering by less than 1.5 Å rmsd). Generally, the top clusters (i.e. those with the most favorable ΔG_{bind}) were also associated with the highest frequency of occurrence, which suggests a good convergence behavior of the search algorithm. Although the predicted free energy of binding is a useful descriptor of ligand/receptor complementarity, the choice of the "best" docking model was ultimately dictated also by its agreement with the SARs data.

For compound **1**[19] (Chart 2), no clear information are available about the absolute configuration at the C-3 carbon of the bicyclic isochromane-based ring system. Moreover, such a system contains a nonaromatic six-membered ring adopting an envelope conformation with the C-3 carbon placed above or below the plane of the ring. According to our calculations, both 3-substituents in **1** can adopt pseudoequatorial and pseudoaxial positions, resulting in two different isoenergetic conformers. Therefore, we decided to subject to docking calculations both conformers of (*R*)-**1** and (*S*)-**1**. As noted above, the SARs indicated that the protonated nitrogen of the ligand had to establish a salt bridge with the Asp130 carboxylate group, but none of the docking experiments, using the conformers with the ethylamine function in pseudoequatorial disposition of both (*R*)-**1** and (*S*)-**1**, produced any ligand orientation with salt bridge motifs in agreement with SAR data. Similarly, for compound (*S*)-**1** having the ethylamine in the pseudoaxial position, AutoDock did not converge toward to a highly populated cluster. On the other hand, most of the results had an unfavorable free energy of binding, thus suggesting that this conformer was not able to find a stable position in the binding site. More encouraging results were achieved for compound (*R*)-**1**, displaying the ethylamine in the pseudoaxial position. In fact, the solution with the lowest free energy of binding ($\Delta G_{bind} = -8.49$ kcal/mol) was found 15 times out of 50. As illustrated in Figure 6A, the positively charged ethylamine moiety of the ligand establishes a salt bridge with the negatively charged carboxylate group of Asp130. Furthermore, the *p*-chlorophenyl ring in position 3 is embedded within a hydrophobic cleft, corresponding to that of P5U Tyr8, which is formed by His208 (ELII), Leu212 (TMV), Trp277 (TMVI), Gln278 (TMVI), and Ala281 (TMVI), where it engages a π-stacking interaction with the indole ring of Trp277. This charge-transfer interaction

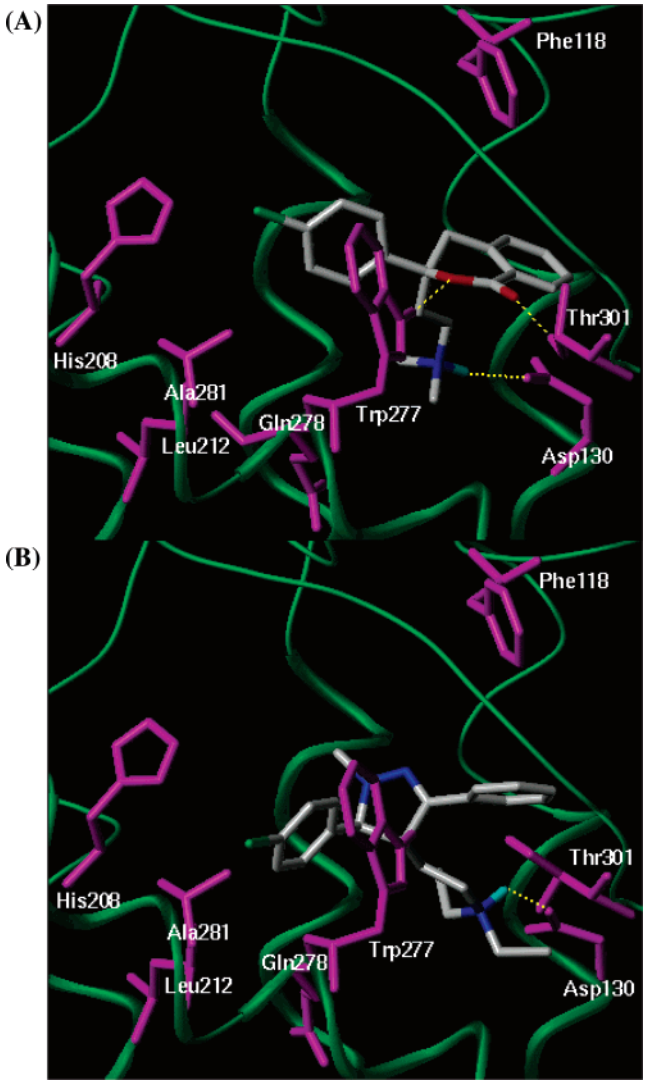

Figure 6. Docked structures of agonists **1** (A) and **2** (B) in the *h*-UTR. The ligands are displayed in white, and key binding site residues are shown in magenta. Hydrogen bonds are represented with dashed yellow lines.

is further stabilized by a hydrogen bond involving the indole NH$^{\epsilon}$ hydrogen of Trp277 and the ester oxygen atom of the isochromanone ring. In addition, the carbonyl oxygen of this ring accepts an additional hydrogen bond from Thr301 (TMVII). Moreover, the benzo-fused

ring of (*R*)-**1** forms a T-shaped interaction with the Phe118 (ELI) aromatic ring.

Since the stereochemistry of the major isomer of **2** was confirmed through NOESY experiments as having an anti configuration,[20] we decided to consider for docking only the (4*R*,5*S*)- and (4*S*,5*R*)-isomers. As regards the (4*R*,5*S*)-stereoisomer, automated docking revealed the preference for a single position in the binding pocket: the result with the top binding energy (−8.72 kcal/mol) was found 44 times out of 50. As shown in Figure 6B, the protonated amino group of (4*R*,5*S*)-**2** forms a salt bridge with the negatively charged carboxylate group of Asp130 in TMIII. Moreover, the *p*-chlorophenyl moiety fits into the same cleft of Tyr8 of P5U, making hydrophobic interactions. In particular, this ring is optimally oriented for a favorable π-stacking interaction with Trp277 (TMVI). Such an interaction is further strengthened by the electron-withdrawing chlorine atom in position 4. In addition, the phenyl ring in position 3 makes contact with the receptor through a T-shaped interaction with Phe118 (ELI). This presents a plausible mode of interaction and could eventually explain the high potency of compound **2** observed experimentally. The preference for a single binding position is even clear in case of the (4*S*,5*R*)-isomer. In fact, the top-ranked cluster had a binding free energy of −8.73 kcal/mol and it was found 18 times out of 50. However, this result was discarded, since the positively charged amino group of **2** was too far away for a significant interaction with the Asp130 carboxylate group.

For benzothiazepine **3**, the anti stereoisomer was synthesized and its potency was evaluated.[20] Since the benzothiazepine ring can exist in two interconverting conformers with the dietylaminoethyl moiety in pseudoaxial or pseudoequatorial position, both conformers of (*R*,*R*)-**3** and (*S*,*S*)-**3** were subjected to the automatic docking calculations. None of the investigated conformers showed the crucial interaction between the positively charged amino group and the negatively charged carboxylate of Asp130 in the docked binding modes, with the exception of (*R*,*R*)-**3** holding the diethylaminoethyl moiety in the pseudoaxial conformation (Figure 7A). In the most frequently occurring and most favorable result (reported in Table 2), the ligand has its *p*-chlorophenyl system placed in the same hydrophobic cleft of Tyr8 of **P5U**, still establishing a π-stacking charge-transfer interaction with the indole ring of Trp277. In addition, the Tyr118 side chain contacts the pendant phenyl ring in position 4 of the ligand via a π-stacking interaction, thus contributing to further stabilize the ligand/receptor complex.

Since the pyrimidinone derivative **4** was synthesized as racemic mixture,[20] both (*R*)- and (*S*)-enantiomers were subjected to the automated docking calculations. As regards the (*R*)-isomer, the most favorable result, which has an estimated ΔG of −7.83 kcal/mol, places the positively charged amino group near the negatively charged carboxylate of Asp130, thus establishing a salt bridge (Figure 7B). The *p*-chlorophenyl ring in position 4 is properly positioned in a hydrophobic cleft formed by the His208, Leu212, Ala281, Trp277, and Gln278 side chains, where it forms an aromatic−aromatic interaction with the Trp277 indole ring. The pendant phenyl ring in position 6 is involved in a T-shaped interaction with the Phe118 aromatic ring in ELI. For the *S*-isomer, a well-defined binding position is also predicted by AutoDock (ΔG_{bind} = −7.78 kcal/mol) but, as occurs for the dihydropyrazole derivative **2**, it is characterized by the absence of the crucial interaction between the protonated amino nitrogen and the Asp130 carboxylate group.

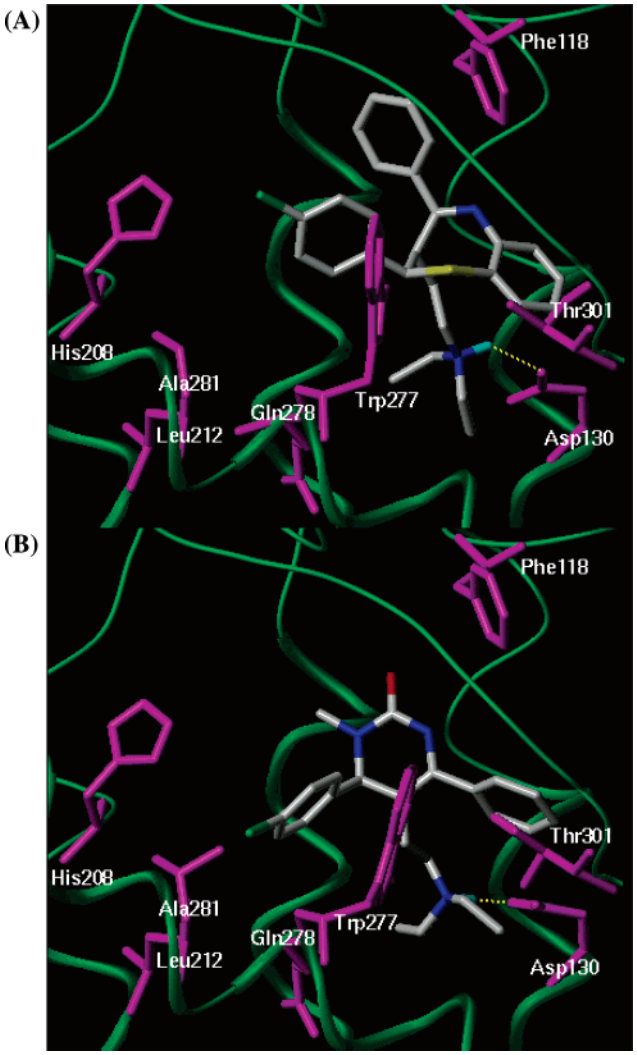

Figure 7. Docked structures of agonists **3** (A) and **4** (B) in the *h*-UTR. The ligands are displayed in white, and key binding site residues are shown in magenta. Hydrogen bonds are represented with dashed yellow lines.

Conclusions

A three-dimensional model of the transmembrane domain of *h*-UTR was carefully built using the crystallographic structure of *b*-Rho as a template to obtain information on the receptor/ligand interactions at the putative ligand binding site and, thus, to facilitate the design of novel lead compounds for current UII drug discovery. The model was thoroughly validated using MD analyses simulations, obtaining results about structural features that are consistent with experimental information. In future studies, this model could be embedded in a phospholipid bilayer[45] to explore, by means of an extensive MD simulation, the allowed conformation and to gain insight into the mechanism of activation.

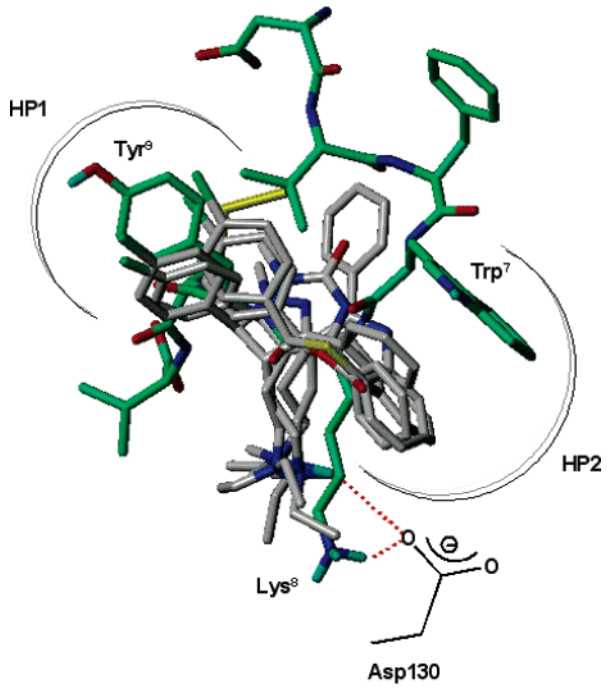

Figure 8. Overlay of the receptor-bound conformations of peptide P5U (green) and non-peptide ligands **1**−**4** (by-atom). The protonated nitrogen of the ligands forms an ion pair with Asp130 in TMIII. HP1 and HP2 map hydrophobic interactions.

The resulting protein structure showing a good steric quality was used to dock the highly active peptide agonist P5U and the non-peptide agonists **1**−**4** into the putative binding site. A crucial anchoring point constituted by Asp130 in TMIII was the starting position for the manual docking of peptide P5U. The key peptide residues Trp7, Lys8, and Tyr9 of P5U, identified as being important for biological function, were found to have significant interactions with the GPCR model. In particular, the protonated ϵ-amino group of Lys8 forms a salt bridge to the negatively charged carboxylate group of Asp130; the aromatic ring of Tyr9 is hosted in a hydrophobic pocket, where it makes specific aromatic−aromatic interactions; and the indole system of Trp7 is still sited in a large hydrophobic cleft, where the indole NH engages a hydrogen bond with the backbone CO of Tyr298.

The molecular recognition of *h*-UTR was further probed by automated docking experiments of non-peptide compounds **1**−**4** and correlated with their low EC_{50} values. For all inspected ligands feasible binding modes were obtained. An overlay of the putative receptor-bound conformations of P5U and compounds **1**−**4** is depicted in Figure 8. When viewing the comparisons, certain specific points of match become apparent: (i) the protonated amino group of **1**−**4** fits well with the P5U Lys8 protonated amino group, all interacting with Asp130 through a salt bridge linkage; (ii) the *p*-clorophenyl ring of non-peptide ligands is superimposed on the peptide Tyr9 aromatic ring, all occupying the hydrophobic pocket HP1; (iii) the benzo-fused aromatic rings of **1** and **3** together with the pendant phenyl rings of **2** and **4** match the peptide Trp7 indole ring, all projecting into the large hydrophobic cleft HP2.

These results suggest that the *h*-UTR may contain an important recognition site in the receptor cavity for the message sequence Trp7, Lys8, and Tyr9 of P5U and UII-related peptides. These amino acids represent the chemical key features, which, in the correct spatial arrangement, are the prerequisite for binding and activation of UTR. Similarly, the non-peptide UII agonists **1**−**4** are able to recognize and activate the receptor, mimicking the three message sequence residues. Taken together, such results delineate the prominent features of a UII agonist pharmacophore, which might be a useful tool in designing novel and potent *h*-UTR ligands.

Computational Methods

Molecular modeling and graphics manipulations were performed using the SYBYL 6.9 software package,[25] running on a Silicon Graphics R12000 workstation. Energy minimizations and MD simulations were realized by employing the AMBER 4.1 program,[46,47] selecting the all-atom Cornell et al. force field.[48]

Human Urotensin Receptor Model. The structural model of the *h*-UTR was built using the recently reported 2.8 Å crystal structure of *b*-Rho[21] (PDB entry code 1F88) as a structural template. Briefly, the *h*-UTR sequence was retrieved from the SWISS-PROT database[49] and aligned with the sequence of *b*-Rho using CLUSTALW software.[50,51] As a first approach, the length of the each α-helix in *h*-UTR was decided after looking for a consensus between the predictions of transmembrane segments provided by SWISS-PROT,[52] as well as by considering that Arg and Lys residues are often located at the membrane boundaries.[53] Extension of each helix was contemplated by taking into account the experimental length of the *b*-Rho helices and the secondary structure prediction of *h*-UTR obtained with the PHD software,[54] as well as the sequence conservation in the possible extensions of the helices (Figure 2).

Individual TM helical segments were built as ideal helices (using $\phi\angle\psi$ angles of −63.0° and −41.6°) with side chains placed in prevalent rotamers and representative proline kink geometries. Each model helix was capped with an acetyl group at the N-terminus and an *N*-methyl group at the C-terminus. These structures were then grouped by adding one at a time until a helical bundle (TM region), matching the overall characteristics of the crystallographic structure of *b*-Rho, had been obtained. The relative orientations and interactions between the helices were adjusted on the basis of incorporated structural inferences from available experimental data, such as mutation and ligand binding studies,[55−57] cysteine scanning data,[58−62] and site-directed mutation experiments.[63−65] Because earlier work showed that polarity conserved positions cluster together in the cores of proteins to create conserved hydrogen-bonding interactions,[66] we refined the model by applying the additional hydrogen-bonding constraints between the conserved polar residues Asn69, Asp97, and Asn311 in accordance with data from site-directed mutagenesis.[63−65]

Homologues for the three extracellular loops were identified using a database of loop fragments[67,68] in SYBYL and the criterion of good geometric fit to the anchor region of the modeled protein. As a more stringent requirement, the loops identified also had to be located between two helices in the template structure. CLUSTALW was then used to determine which of the loop fragments that met this criterion had the highest homology with the *h*-UTR loop sequences. PSI-BLAST[69,70] was also used in an attempt to identify the loop regions; however, no hits were found with an *E*-value greater than 0.01, probably because the sequences were too short. When looser constraints were used, the highest scoring sequences were not of loop regions. Hence, the SYBYL loop search results were used. The loops were positioned with their N and C termini approximately equidistant from the two end residues of the helices to which they were to be connected (in all cases, the distance between the loop ends differed by ≤1 Å from the distance between the target helices). A peptide bond was then formed with the "join chain" function in SYBYL, and

the six residues surrounding the new bond were minimized. Moreover, the disulfide bridge between Cys123 (ELI) and Cys199 (ELII) was included throughout all calculations.

After all connections were made, the whole structure was energy-minimized using the SANDER module of the AMBER suite of programs until the rmsd value of the conjugate gradient was 0.001 kcal/mol per Å. To avoid spurious changes in the general fold and helix packing due to some still unfavorable electrostatic interactions or steric clashes, an energy penalty force constant of 10 kcal/Å^2/mol on the protein backbone atoms was applied throughout these calculations.

The model obtained for the seven-helix bundle of the *h*-UTR was then used as the starting point for subsequent 300 ps of MD simulations. The options of MD at 300 K with 0.2 ps coupling constant were a time step of 1 fs and a nonbonded update every 25 fs. The lengths of bonds with hydrogen atoms were constrained according to the SHAKE algorithm.[71] When MD simulations are performed in the gas phase, disregarding the explicit macroscopic environment necessitates the use of a set of restraints, replacing the natural stabilizing effects of the membrane bilayer on helix length and packing. According to SYBYL standard parameters, hydrogen bonds, which are found to stabilize the helical conformation, were determined in the backbone of the minimized model. For the first 100 ps, semiharmonic restraints with a force constant of 5.0 kcal/Å^2/mol were applied to these hydrogen bonds in order to preserve the actual interactions between the amide hydrogens and the carbonyl oxygens. The harmonic part of the restraint was set to change into a linear gradient below 0.8 Å and above 2.8 Å hydrogen-bond distance. After 100 ps, the force constant was gradually reduced to 0.05 kcal/Å^2/mol over a time period of 100 ps, allowing the system to relax. According to preliminary studies about the optimal simulation setup (data not shown), for the remaining 100 ps we decided to refrain from decreasing the force constant below this value to maintain the original structural information contained in the crystal structure of bovine rhodopsin. The average structure from the last 50 ps trajectory of MD was reminimized until a rms of 0.5 kcal/mol per Å was reached. The harmonic restraints were gradually lowered in steps of 5 kcal/mol, minimizing the structure at each step until a rms of 0.5 kcal/mol per Å was reached. When the restraints were finally removed, the structure was submitted to the final energy minimization until a rms of 0.001 kcal/mol per Å was reached.

The conformational validity of main chain and side chain torsions in each residue within the protein model was analyzed using the PROCHECK program.[36,37] Also, all ω angles for the peptide planarity were measured. The chirality of all Cα atoms, which in naturally occurring amino acids is of the L-configuration, was checked. Root mean square deviations between backbone atoms in all helices were compared to the X-ray structure of *b*-Rho as a template.

Docking Simulations. The peptide P5U was manually docked in the suspected binding site of the receptor by maximizing the electrostatic interactions. The highly conserved Asp130 on TMIII, mentioned in Results and Discussion, was assumed to participate in the binding. Thus, the positively charged Lys8 of the ligand was positioned in such a way to interact with the carboxylate group of Asp130. The resulting complex was selected on the basis of the SARs available at that time. The receptor model with the best-defined pockets for the other two key side chains of P5U, Trp7 and Tyr9, was chosen as working model.

As concerns the non-peptide ligands **1**−**4**, docking was performed with version 3.05 of the AutoDock software package.[43,44] It combines a rapid energy evaluation through precalculated grids of affinity potentials with a variety of search algorithms to find suitable binding positions for a ligand on a given protein. While the protein is required to be rigid, the program allows torsional flexibility in the ligand. Docking to *h*-UTR was carried out using the empirical free energy function and the Lamarckian genetic algorithm, applying a standard protocol, with an initial population of 50 randomly placed individuals, a maximum number of 1.5×10^6 energy evaluations, a mutation rate of 0.02, a cross-over rate of 0.80, and an elitism value of 1. Proportional selection was used, where the average of the worst energy was calculated over a window of the previous 10 generations. For the local search, the so-called pseudo-Solis and Wets algorithm was applied using a maximum of 300 iterations per local search. The probability of performing the local search on an individual in the population was 0.06, and the maximum number of consecutive successes or failures before doubling or halving the local search step size was 4. Fifty independent docking runs were carried out for each ligand. Results differing by less than 1.5 Å in positional rmsd were clustered together and represented by the result with the most favorable free energy of binding.

(1) Ligand Setup. The core structures of ligands **1**−**4** were retrieved from the Cambridge Structural Database (CSD)[72] and modified using standard bond lengths and bond angles of the SYBYL fragment library. Geometry optimizations were realized with the SYBYL/MAXIMIN2 minimizer by applying the BFGS (Broyden, Fletcher, Goldfarb, and Shannon) algorithm[73] and setting a rms gradient of the forces acting on each atom of 0.05 kcal/mol Å as the convergence criterion. Atomic charges were assigned using the Gasteiger−Marsili formalism,[74] which is the type of atomic charges used in calibrating the AutoDock empirical free energy function. Finally, the two compounds were set up for docking with the help of AutoTors, the main purpose of which is to define the torsional degrees of freedom to be considered during the docking process. The number of flexible torsions defined for each ligand is four for **1** and nine for **2**−**4**.

(2) Protein Setup. The energy-minimized structure of *h*-UTR model was set up for docking as follows: polar hydrogens were added using the biopolymers module of the SYBYL program, (Arg, Lys, Glu, and Asp residues were considered ionized, while all His were considered neutral by default), and Kollman united-atom partial charges were assigned. Solvation parameters were added to the final protein file using the Addsol utility of AutoDock. The grid maps representing the proteins in the actual docking process were calculated with AutoGrid. The grids (one for each atom type in the ligand, plus one for electrostatic interactions) were chosen to be sufficiently large to include not only the active site but also significant portions of the surrounding surface. The dimensions of the grids were thus 50 Å × 40 Å × 40 Å, with a spacing of 0.375 Å between the grid points.

MD Simulations. Refinement of the P5U/*h*-UTR bound complex was achieved by in vacuo energy minimization with the SANDER module of AMBER (50 000 steps; distance dependent dielectric function of $\epsilon = 4r$), by applying an energy penalty force constant of 5 kcal/mol on the protein backbone atoms. The geometry-optimized complex was then used as the starting point for subsequent 400-ps MD simulation, during which the positional constraints on the protein backbone were gradually reduced from 5 to 0.1 kcal Å^{-2} mol^{-1}. The additional parameters required for the ligands were derived by analogy to existing parameters. Partial atomic charges for the ligands were imported from the output files of AM1 full geometry optimizations as implemented in the MOPAC 6.0 program.[75,76] A time step of 1 fs and a nonbonded pairlist updated every 25 fs were used for the MD simulations. The temperature was maintained at 300 K using the Berendsen algorithm[77] with a 0.2 ps coupling constant. An average structure was calculated from the last 100 ps trajectory and energy-minimized using the steepest descent and conjugate gradient methods as specified above. The MD trajectories were analyzed by means of the CARNAL module of AMBER package.

Acknowledgment. This work was supported by a grant from Ministero dell'Università e della Ricerca Scientifica.

References

(1) Bern, H. A.; Pearson, D.; Larson, B. A.; Nishioka, R. S. Neurohormones from fish tails: The caudal neurosecretory system. I. 'Urophysiology' and the caudal neurosecretory system of fishes. *Recent Prog. Horm. Res.* **1995**, *41*, 533−552.

(2) Coulouarn, Y.; Lihrmann, I.; Jegou, S.; Anouar, Y.; Tostivint, H.; Beauvillain, J. C.; Conlon, J. M.; Bern, H. A.; Vaudry, H. Cloning of the cDNA encoding the urotensin II precursor in frog and human reveals intense expression of the urotensin II gene in motoneurons of the spinal cord. *Proc. Natl. Acad. Sci. U.S.A.* **1998**, *95*, 15803−15808.
(3) Ames, R. S.; Sarau, H. M.; Chambers, J. K.; Willette, R. N.; Aiyar, R. V.; Romanic, A. M.; Louden, C. S.; Foley, J. J.; Sauermelch, C. F.; Coatney, R. W.; Ao, Z.; Disa, J.; Holmes, S. D.; Stadel, J. M.; Martin, J. D.; Liu, W.-S.; Glover, G. I.; Wilson, S.; McNutty, D. E.; Ellis, C. E.; Eishourbagy, N. A.; Shabon, U.; Trill, J. J.; Hay, D. V. P.; Ohlstein, E. H.; Bergsma, D. J.; Douglas, S. A. Human urotensin-II is a potent vasoconstrictor and agonist for the orphan receptor GPR14. *Nature* **1999**, *401*, 282−286.
(4) Coulouarn, Y.; Jegou, S.; Tostivint, H.; Vaudry, H.; Lihrmann, I. Cloning, sequence analysis and tissue distribution of the mouse and rat urotensin II precursors. *FEBS Lett.* **1999**, *457*, 28−32.
(5) Davenport, A. P.; Maguire J. J. Urotensin II: Fish neuropeptide catches orphan receptor. *Trends Pharmacol. Sci.* **2000**, *21*, 80−82.
(6) Nothacker, H. P.; Wang, Z.; McNeill, A. M.; Saito, Y.; Merten, S.; O'Dowd, B.; Duckles, S. P.; Civelli, O. Identification of the natural ligand of an orphan G-protein coupled receptor involved in the regulation of vasoconstriction. *Nat. Cell Biol.* **1999**, *1*, 383−385.
(7) Conlon, J. M.; Yano, K.; Waugh, D.; Hazon, N. Distribution and molecular forms of urotensin II and its role in cardiovascular regulation in vertebrates. *J. Exp. Zool.* **1996**, *275*, 226−238.
(8) Böhm, F.; Pernow, J. Urotensin II evokes potent vasoconstriction in human in vivo. *Br. J. Pharmacol.* **2002**, *135*, 25−27.
(9) Douglas, S. A.; Ohlstein, E. H. Human urotensin-II, the most potent mammalian vasoconstrictor identified to date, as a therapeutic target for the management of cardiovascular diseases. *Trends Cardiovasc. Med.* **2000**, *10*, 229−237.
(10) MacLean, M. R.; Alexander, D.; Stirrat, A.; Gallagher, M.; Douglas, S. A.; Ohlstein, E. H.; Morecroft, I.; Polland, K. Contractile responses to human urotensin-II in rat and human pulmonary arteries: Effect of endothelial factors and chronic hypoxia in the rat. *Br. J. Pharmacol.* **2000**, *130*, 201−204.
(11) Russell, F. D.; Molenaar, P.; O'Brien, D. M. Cardiostimulant effects of urotensin-II in human heart in vitro. *Br. J. Pharmacol.* **2001**, *132*, 5−9.
(12) Zou, Y.; Nagai, R.; Yamazaki, T. Urotensin II induces hypertrophic responses in cultured cardiomyocytes from neonatal rats. *FEBS Lett.* **2001**, *8*, 57−60.
(13) Watanabe, T.; Koba, S.; Katagiri, T.; Pakala, R.; Benedict, C. R. Lysophosphatidylcholine potentiates the mitogenic effect of various vasoactive compounds on rabbit aortic smooth muscle cells. *Jpn. Heart J.* **2002**, *43*, 409−416.
(14) Marchese, A.; Heiber, M.; Nguyen, T.; Heng, H. H.; Saldivia, V. R.; Cheng, R.; Murphy, P. M.; Tsui, L. C.; Shi, X.; Gregor, P.; George, S. R.; O'Dowd, B. F.; Doehrty, J. M. Cloning and chromosomal mapping of three novel genes, GPR9, GPR10 and GPR14, encoding receptor related to interleukin 8, neuropeptide Y, and somatostatin receptors. *Genomics* **1995**, *29*, 335−344.
(15) Brkovic, A.; Hattenberger, A.; Kostenis, E.; Klabunde, T.; Flohr, S.; Kurz, M.; Bourgault, S.; Fournier, A. Functional and binding characterizations of urotensin II-related peptides in human and rat urotensin II-receptor assay. *J. Pharmacol. Exp. Ther.* **2003**, *306*, 1200−1209.
(16) Flohr, S.; Kurz, M.; Kostenis, E.; Brkovich, A.; Fournier, A.; Klabunde, T. Identification of nonpeptidic urotensin II receptor antagonists by virtual screening based on a pharmacophore model derived from structure−activity relationships and nuclear magnetic resonance studies on urotensin II. *J. Med. Chem.* **2002**, *45*, 1799−1805.
(17) Camarda, V.; Rizzi, A.; Calò, G.; Gendron, G.; Perron, S. I.; Kostenis, E.; Zamboni, P.; Mascoli, F.; Regoli, D. Effects of human urotensin II in isolated vessels of various species; comparison with other vasoactive agents. *Naunyn-Schmiedeberg's Arch. Pharmacol.* **2002**, *365*, 141−149.
(18) Grieco, P.; Carotenuto, A.; Campiglia, P.; Zampelli, E.; Patacchini, R.; Maggi, C. A.; Novellino, E.; Rovero, P. A new potent urotensin-II receptor peptide agonist containing a Pen residue at disulfide bridge *J. Med. Chem*. **2002**, *45*, 4391−4394.
(19) Croston, G. E.; Olsson, R.; Currier, E. A.; Burstein, E. S.; Weiner, D.; Nash, N.; Severance, D.; Allenmark, S. G.; Thunberg, L.; Ma, J. N.; Mohell, N.; O'Dowd, B.; Brann, M. R.; Hacksell, U. Discovery of the first nonpeptide agonist of the GPR14/urotensin-II receptor: 3-(4-Chlorophenyl)-3-(2-(dimethylamino)ethyl)isochroman-1-one (AC-7954). *J. Med. Chem*. **2002**, *45*, 4950−4953.
(20) Olsson, R. PCT Int. Appl. 2004, 29 pp WO 2004073642 A2 20040902.
(21) Palczewski, K.; Kumasaka, T.; Hori, T.; Behnke, C. A.; Motoshima, H.; Fox, B. A.; Le Trong, I.; Teller, D. C.; Okada, T.; Stenkamp, T. E.; Yamamoto, M.; Miyano, M. Crystal Structure of Rhodopsin: A G Protein-Coupled Receptor. *Science* **2000**, *289*, 739−745.
(22) Ballesteros, J.; Palczewski, K. G protein-coupled receptor drug discovery: Implications from the crystal structure of rhodopsin. *Curr. Opin. Drug Discovery Dev.* **2001**, *4*, 561−574.
(23) Ballesteros, J. A.; Shi, L.; Javitch, J. A. Structural mimicry in G protein-coupled receptors: Implications of the high-resolution structure of rhodopsin for structure−function analysis of rhodopsin-like receptors. *Mol. Pharmacol.* **2001**, *60*, 1−19.
(24) Bissantz, C.; Bernard, P.; Hibert, M.; Rognan, D. Protein-based virtual screening of chemical databases. II. Are homology models of G-Protein Coupled Receptors suitable targets? *Proteins* **2003**, *50*, 5−25.
(25) *SYBYL Molecular Modelling System*, version 6.9.1; Tripos Inc.: St. Louis, MO, 2003.
(26) Lerche, M. H.; Kragelund, B. B.; Bech, L. M.; Poulsen, F. M. Barley lipid-transfer protein complexed with palmitoyl CoA: The structure reveals a hydrophobic binding site that can expand to fit both large and small lipid-like ligands. *Structure* **1997**, *5*, 291−306.
(27) Grimes, J.; Basak, A. K.; Roy, P.; Stuart, D. The crystal structure of bluetongue virus VP7. *Nature* **1995**, *373*, 167−170.
(28) Izard, T.; Lawrence, M. C.; Malby, R. L.; Lilley, G. G.; Colman, P. M. The three-dimensional structure of *N*-acetylneuraminate lyase from *Escherichia coli*. *Structure* **1994**, *2*, 361−369.
(29) Mirzadegan, T.; Benko, G.; Filipek, S.; Palczewski, K. Sequence analyses of G-protein-coupled receptors: Similarities to rhodopsin. *Biochemistry* **2003**, *42*, 2759−2767.
(30) Farrens, D. L.; Altenbach, C.; Yang, K.; Hubbell, W. L.; Khorana, H. G. Requirement of rigid-body motion of transmembrane helices for light activation of rhodopsin. *Science* **1996**, *274*, 768−770.
(31) Dunham, T. D.; Farrens, D. L. Conformational changes in rhodopsin- Movement of helix F detected by site-specific chemical labeling and fluorescence spectroscopy. *J. Biol. Chem.* **1999**, *274*, 1683−1690.
(32) Jensen, A. D.; Guarnieri, F.; Rasmussen, S. G. F.; Asmar, F.; Ballesteros, J. A.; Gether, U. Agonist-induced conformational changes at the cytoplasmatic side of transmembrane segment 6 in the β_2 adrenergic receptor mapped by site-selective fluorescent labeling. *J. Biol. Chem.* **2001**, *276*, 9279−9290.
(33) Lin, S. W.; Sakmar, T. P. Specific tryptophan UV-absorbance changes are probes of the transition of rhodopsin to its active state. *Biochemistry* **1996**, *35,* 1149−11159.
(34) Nikiforovich, G. V.; Marshall, G. R. Three-dimensional model for meta-II rhodopsin, an activated G-protein-coupled receptor. *Biochemistry* **2003**, *42*, 9110−9120.
(35) Gouldson, P. R.; Kidley, N.; Bywater, R. P.; Psaroudakis, G.; Brooks, H. D.; Diaz, C.; Shire, D.; Reynolds, C. A. Towards the active conformations of rhodopsin and the Beta-2-adrenergic receptors. *Proteins Struct. Funct. Genet. Bioinformat.* **2004**, *56*, 67−84.
(36) Laskowski, R. A.; MacArthur, M. W.; Moss, D. S. Thornton. J. M. PROCHECK: A Program to Check the Stereochemical Quality of Protein Structures. *J. Appl. Crystallogr.* **1993**, *26*, 283−291.
(37) Morris, A. L.; MacArthur, M. W.; Hutchinson, E. G.; Thornton, J. M. Stereochemical Quality of Protein Structure Coordinates. *Proteins* **1992**, *12*, 345−364. *Chem.* **1994**, *15*, 162−182.
(38) Colson, A.-O.; Perlman, J. H.; Jinsi-Parimoo, A.; Nussenzveig, D. R.; Osman, R.; Gershengorn, M. C. A hydrophobic cluster between transmembrane helices 5 and 6 constrains the thyrotropin-releasing hormone receptor in an inactive conformation. *Mol. Pharmacol*. **1998**, *54*, 968−978.
(39) Strader, C. D.; Candelore, M. R.; Hill, W. S.; Sigal, I. S.; Dixon, R. A. F. Identification of two serine residues involved in agonist activation of the β-adrenergic receptor. *J. Biol. Chem.* **1989**, *264*, 13572−13578.
(40) Strader, C. D.; Gaffney, T.; Sugg, E. E.; Rios Candelore, M.; Keys, R.; Patchett, A. A.; Dixon, R. A. F. Allele-specific activation of genetically engineered receptors. *J. Biol. Chem.* **1991**, *266*, 5−8.
(41) Kinney, W. A.; Almond, H. R., Jr.; Qi, J.; Smith, C. E.; Santulli, R. J.; de Garavilla, L.; Andrade-Gordon, P.; Cho, D. S.; Everson, A. M.; Feinstein, M. A.; Leung, P. A.; Maryanoff, B. E. Structure−Function Analysis of Urotensin II and Its Use in the Construction of a Ligand−Receptor Working Model. *Angew. Chem., Int. Ed.* **2002**, *41*, 2940−2944.
(42) Itoh, H.; Itoh, Y.; Rivier, J.; Lederis, K. Contraction of major artery segments of rat by fish neuropeptide urotensin II. *Am. J. Physiol.* **1987**, *252*, R361−R366.
(43) Morris, G. M.; Goodsell, D. S.; Halliday, R. S.; Huey, R.; Hart, W. E.; Belew, R. K.; Olson, A. J. Automated docking using a Lamarckian genetic algorithm and an empirical binding free energy function. *J. Comput. Chem.* **1998**, *19*, 1639−1662.

(44) Goodsell, D. S.; Morris, G. M.; Olson, A. J. Automated docking of flexible ligands: Applications of AutoDock. *J. Mol. Recognit.* **1996**, *9*, 1−5.
(45) Heller, H.; Schaefer, M.; Schulten, K. Molecular dynamics simulation of a bilayer of 200 lipids in the gel and in the liquid-crystal phases. *J. Phys. Chem.* **1993**, *97*, 8343−8360.
(46) Pearlman, D. A.; Case, D. A.; Caldwell, J. W.; Ross, W. S.; Cheatham T. E., III.; Debolt, S.; Ferguson, D. M.; Seibel, G. L.; Kollman, P. A. AMBER, a package of computer programs for applying molecular mechanics, normal-mode analysis, molecular dynamics and free energy calculations to simulate the structural and energetic properties of molecules. *Comput. Phys. Commun.* **1995**, *91*, 1−41.
(47) Pearlman, D. A.; Case, D. A.; Caldwell, J. W.; Ross, W. S.; Cheatham T. E., III.; Ferguson, D. M.; Seibel, G.; Singh, U. C.; Weiner, P. K.; Kollman, P. A. AMBER 4.1; Department of Pharmaceutical Chemistry, University of California: San Francisco, CA, 1995.
(48) Cornell, W. D.; Cieplak, P.; Bayly, C. I.; Gould, I. R.; Merz, K. M.; Ferguson, D. M.; Spellmeyer, D. C.; Fox, T.; Caldwell, J. W.; Kollman, P. A. A Second Generation Force Field for the Simulation of Proteins, Nucleic Acids, and Organic Molecules. *J. Am. Chem. Soc.* **1995**, *117*, 5179−5197.
(49) Bairoch, A.; Apweiler, R. The SWISS-PROT protein sequence database and its supplement TrEMBL in 2000. *Nucleic Acids Res.* **2000**, *28*, 45−48.
(50) Thompson, J. D.; Higgins, D. G.; Gibson, T. J. CLUSTAL W: Improving the sensitivity of progressive multiple sequence alignment through sequence weighting, position-specific gap penalties and weight matrix choice. *Nucleic Acids Res.* **1994**, *22*, 4673−4680.
(51) CLUSTAL W (version 1.82): http://www.ebi.ac.uk/clustalw/ (default settings: matrix, PAM250 series; gap opening penalty, 10; gap extension penalty, 0.05).
(52) SWISS-PROT is available online at http://us.expasy.org.
(53) Ballesteros, J. A.; Weinstein, H. W. Integrated methods for the construction of three-dimensional models and computational probing of structure−function relations in G-protein coupled receptors. In *Methods in Neuroscience*; Sealfon, S. C., Ed.; Academic Press: San Diego, 1995; pp 366−428.
(54) Rost, B.; Sander, C. Prediction of protein secondary structure at better than 70% accuracy. *J. Mol. Biol.* **1993**, *232*, 584−599.
(55) Baldwin, J. M. Structure and function of receptors coupled to G proteins. *Curr. Opin. Cell. Biol.* **1994**, *6*, 180−190.
(56) Schwartz, T. W. Locating ligand-binding sites in 7TM receptors by protein engineering. *Curr. Opin. Biotechnol.* **1994**, *5*, 434−444.
(57) van Rhee, A. M.; Jacobson, K. A. Molecular architecture of G protein-coupled receptors. *Drug Dev. Res.* **1996**, *37*, 1−38.
(58) Javitch, J. A.; Li, X.; Kaback, J.; Karlin, A. A Cysteine residue in the third membrane-spanning segment of the human D2 dopamine receptor is exposed in the binding-site crevice. *Proc. Natl. Acad. Sci. U.S.A.* **1994**, *91*, 10355−10359.
(59) Javitch, J. A.; Fu, D. Y.; Chen, J. Y.; Karlin, A. Residues in the fifth membrane-spanning segment of the dopamine D2 receptor exposed in the binding-site crevice. *Biochemistry* **1995**, *34*, 16433−16439.
(60) Javitch, J. A.; Fu, D.; Liapakis, G.; Chen, J. Constitutive activation of the beta2 adrenergic receptor alters the orientation of its sixth membrane-spanning segment. *J. Biol. Chem.* **1997**, *272*, 18546−18549.
(61) Fu, D.; Ballesteros, J. A.; Weinstein, H.; Chen, J.; Javitch, J. A. Residues in the seventh membrane-spanning segment of the dopamine D2 receptor accessible in the binding-site crevice. *Biochemistry* **1996**, *35*, 11278−11285.
(62) Xu, W.; Li, J.; Chen, C.; Huang, P.; Weinstein, H.; Javitch, J. A.; Shi, L.; De Riel, J. K.; Liu Chen, L. Y. Comparison of the amino acid residues in the sixth transmembrane domains accessible in the binding-site crevices of mu, delta, and kappa opioid receptors. *Biochemistry* **2001**, *40*, 8018−8029.
(63) Perlman, J. H.; Colson, A. O.; Wang, W.; Bence, K.; Osman R.; Gershengorn, M. C. Interactions between conserved residues in transmembrane helices 1, 2, and 7 of the tyrotropin-releasing hormone receptor. *J. Biol. Chem.* **1997**, *272*, 11937−11942.
(64) Sealfon, S. C.; Chi, L.; Eversole, B. J.; Rodic, V.; Zhang, D.; Ballesteros, J. A.; Weinstein, H. Related contribution of specific helix 2 and 7 residues to conformational activation of the serotonin 5-HT_{2a} receptor. *J. Biol. Chem.* **1995**, *270*, 16683−16688.
(65) Zhou, W.; Flanagan, C. A.; Ballesteros, J.; Konvicka, K.; Davidson, J. S.; Weinstein, H.; Millar, R. P.; Sealfon, S. C. A reciprocal mutation supports helix 2 and helix 7 proximity in the gonadotropin-releasing hormone receptor. *Mol. Pharmacol.* **1994**, *45*, 165−170.
(66) Zhang, D.; Weinstein, H. Polarity conserved positions in transmembrane domains of G-protein coupled receptors and bacteriorhodopsin. *FEBS Lett.* **1994**, *337*, 207−212.
(67) Jones, T. A.; Thirup, S. Using known substructures in protein model-building and crystallography. *EMBO J.* **1986**, *5*, 819−822.
(68) Claessens, M.; Van Cutsem, E.; Lasters, I.; Wodak, S. Modeling the polypeptide backbone with spare parts from known protein structures. *Protein Eng.* **1989**, *2*, 335−345.
(69) Altschul, S. F.; Madden, T. L.; Schaffer, A. A.; Zhang, J.; Zhang, Z.; Miller, W.; Lipman, D. J. Gapped BLAST and PSI-BLAST: A new generation of protein database search programs. *Nucleic Acids Res.* **1997**, *25*, 3389−3402.
(70) PSI-BLAST: http://www.ncbi.nlm.nih.gov/BLAST/(default settings; matrix, Blosum62).
(71) Ryckaert, J. P.; Ciccotti, G.; Berendsen, H. J. C. Numerical Integration of the Cartesian Equations of motion for a system with constraints: Molecular dynamics of *n*-alkanes. *J. Comput. Phys.* **1977**, *23*, 327−333.
(72) Allen, F. H.; Bellard, S.; Brice, M. D.; Cartwright, B. A.; Doubleday, A.; Higgs, H.; Hummelink, T.; Hummelink-Peters, B. G.; Kennard, O.; Motherwell, W. D. S. The cambridge crystallographic data center: Computer-based search, retrieval, analysis and display of information. *Acta Crystallogr.* **1979**, *B35*, 2331−2339.
(73) Head, J.; Zerner, M. C. A Broyden-Fletcher-Goldfarb-Shanno optimization procedure for molecular geometries. *Chem. Phys. Lett.* **1985**, *122*, 264−274.
(74) Gasteiger, J.; Marsili, M. Iterative partial equilization of orbital electronegativity—A rapid access to atomic charges. *Tetrahedron* **1980**, *36*, 3219−3228.
(75) Dewar, M. J. S.; Zoebisch, E. G.; Healy, E. F.; Stewart, J. J. P. AM1: A new general purpose mechanical molecular model. *J. Am. Chem. Soc.* **1985**, *107*, 3902−3909.
(76) MOPAC (version 6.0) is available from Quantum Chemistry Program Exchange, No. 455.
(77) Berendsen, H. J. C.; Postma, J. P. M.; van Gunsteren, W. F.; DiNola, A.; Haak, J. R. Molecular Dynamics with Coupling to an External Bath. *J. Chem. Phys.* **1984**, *81*, 3684−3690.

JM049110X